Compression of sodium-filled and empty open-framework Si_{24} under quasi- and non-hydrostatic conditions

Thomas B. Shiell and Timothy A. Strobel

Earth and Planets Laboratory, Carnegie Institution for Science, Washington DC, 20015, USA

Isothermal equations of state were determined for the open-framework silicon allotrope Si_{24} and its Na-filled precursor (Na_4Si_{24}) using different pressure media including hydrogen and argon, and with no pressure medium. Si_{24} does not transform into diamond-cubic silicon under compression, and the low-density phase possesses a bulk modulus 91(2) GPa. The Na-filled precursor exhibits a comparable volumetric compressibility with different axial trends that are explained by the crystallographic structure. Above 11 GPa, Si_{24} transforms to the β-tin structure followed other high-pressure silicon allotropes similar to diamond-cubic silicon, driven by a large increase in density. Small molecules like H_2 do not enter the channels of Si_{24} during compression at room temperature, however, hydrostaticity strongly influences the transformation pressure and range of coexistence with other phases including β-Sn, *Imma*, and simple-hexagonal Si.

I. INTRODUCTION

Silicon (Si) is readily abundant in nature and is currently the dominant material in the modern semiconductor and electronics industries. In its most thermodynamically stable form at ambient conditions, Si adopts the diamond cubic structure (DC-Si, $Fd\bar{3}m$, a = 5.431 Å) and has an inherent indirect band gap of 1.1 eV.[1,2] However, this indirect band gap limits the ability of DC-Si to be the major component of next-generation optoelectronic and photonic technologies,[3–6] promoting the search for new materials compatible with current CMOS-technologies and manufacturing processes that have desirable optical and electrical properties.[7]

In recent decades, substantial research effort has been contributed toward the synthesis of other novel stable and metastable forms of Si with potentially useful properties, including improved light absorption and emission. Pure Si allotropes are particularly desirable as they would be relatively easy to incorporate into pre-existing technologies and with well-developed manufacturing processes. Pure Si allotropes that are recoverable to ambient conditions include BC8, R8, and hexagonal diamond (HD)-Si.[8] Other unique allotropes have been produced locally through confined micro-explosions.[9] The BC8-Si structure is a narrow-gap semiconductor,[10,11] while calculations indicate that R8-Si has a small indirect band gap of 0.24 eV.[12] HD-Si has a similar electronic structure to DC-Si,[13] but solid solutions with Ge may offer the possibility for tunable direct band gaps in the near- to mid-infrared.[7,14] While several Si allotropes are already known, calculations indicate that there are numerous others with desirable optical or electrical properties, and additional isolatable crystalline forms are yet to be synthesized.

Si-rich compounds have also been used as viable precursors for synthesizing novel Si allotropes with potentially desirable physical properties.[15] For example, Na–Si clathrate structures such as $Na_{24}Si_{136}$ (Type-II clathrate, cubic $Fd\bar{3}m$) have been synthesized via thermal decomposition [16] and by using high pressure

and temperature.[17,18] Na can be removed from the Type-II structure to produce Si_{136}.[19,20] While Si_{136} has a wide direct (or nearly direct) gap near 2 eV, optically forbidden transitions and difficulties associated with the production of high-quality crystals and films have hindered recent developments.[21,22] Similar to Si_{136}, the open-framework allotrope Si_{24} can be produced by removing Na from the high-pressure precursor Na_4Si_{24} ($EuGa_2Ge_4$-type structure,[23] orthorhombic *Cmcm*, a = 4.081 Å, b = 10.579 Å, c = 12.275 Å).[17,24] Unlike the Si clathrates, which contain polyhedral cages that tile three-dimensional space, Si_{24} is a "clathrate-like" open-framework structure with one-dimensional channels along the crystallographic a-axis [see Fig. 1(a–c)]. This altered geometry allows for increased Na mobility and guest removal at much lower temperatures compared with Type-II clathrate. After Na-removal, the volume of the resulting Si_{24} framework is slightly contracted (orthorhombic *Cmcm*, a = 3.818 Å, b = 10.692 Å, c = 12.637 Å),[25] as shown in Fig. 1(d). Si_{24} possesses a quasi-direct band gap near 1.4 eV, [26,27] close to the ideal band gap for light absorption in the Shockley-Queisser limit for single-junction devices,[28] which suggests potential for efficient conversion of the solar spectrum compared to DC-Si.[27] Recently, large pure single crystals of Si_{24} were demonstrated.[26]

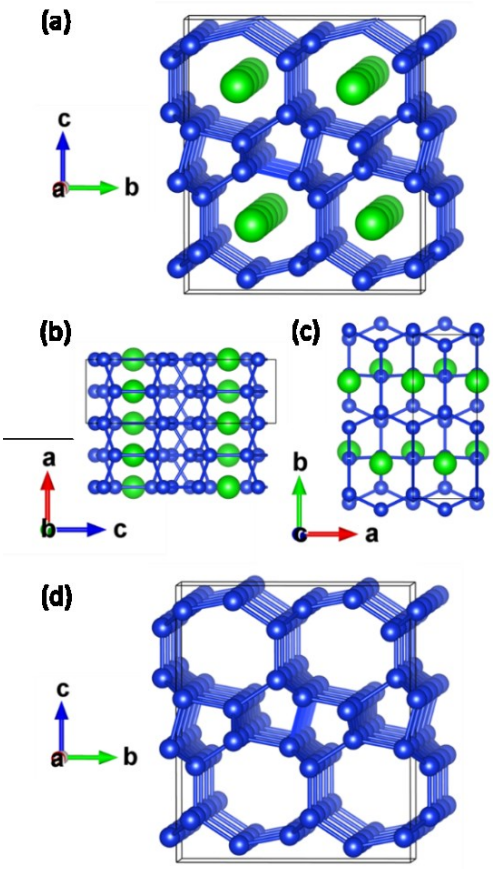

FIG. 1. (a) The structure of Na_4Si_{24} with Na-filled channels shown along the a-axis. The Na atoms are green, and the Si atoms are blue. (b) and (c) show the alternating occupancy of Na atoms in the channel openings viewed along the b and c-axis, respectively. The unit cell is indicated by the black box. (d) The Na-free Si_{24} structure showing the empty channels along the a-axis. These images were generated using VESTA-v3.[29]

While Si_{24} is metastable at ambient conditions and was shown to persist above 700 K,[25] its high-pressure stability, phase transition sequence, and bulk mechanical properties remain unknown. Previous open-framework structures were shown to exhibit anomalous properties such as negative thermal expansion,[30–32] and certain optical phonons of Si_{24} exhibit softening with pressure and negative Grüneisen parameters suggesting potential for anisotropic compression.[33] Previous studies on cubic Si_{136} clathrate demonstrated a surprisingly high bulk modulus compared with DC-Si,[34] but it is unclear whether this structural stability will extend to orthorhombic Si_{24}. In addition, it remains unconfirmed whether small gaseous atoms penetrate into the open-framework channels under pressure – the diameter of the large 8-membered ring is comparable to a He atom or H_2 molecule – similar to observations of other zeolite-type structures.[35–37]

In this paper, we address these open questions by studying compressed Na_4Si_{24} and Si_{24} using *in situ* synchrotron X-ray diffraction (XRD) measurements. We then quantify the mechanical compressibility parameters using a variety of pressure media (PM) and show that hydrostaticity strongly influences the transformation pressure of Si_{24} and its prevalence to coexist with other high-pressure Si phases.

II. METHODS

A. Sample preparation and loading

The Na_4Si_{24} precursor and subsequent Si_{24} samples were prepared as discussed previously.[25,26] In short, a 6:1 molar DC-Si (powder Alfa-Aesar, 99.999%) to Na metal (Alfa-Aesar, 99.95%) mixture was prepared in an Ar glovebox and sealed within a boron nitride capsule for high-pressure synthesis at 9 GPa and 1125 K using a 14/8 multi-anvil assembly.[24] To prepare Si_{24}, recovered Na_4Si_{24} samples were wrapped in a Ta pouch and placed inside a quartz tube under a dynamic vacuum of $3x10^{-5}$ torr. The sample was then annealed at 125°C under vacuum for four days to generate Na-free Si_{24}.[25] The resulting material was sonicated and rinsed in water to remove any residual Na salts on the surface of the Si_{24}.

All high-pressure experiments were performed in diamond anvil cells (DAC) equipped with culets ranging between 500-600 μm in diameter. Re metal gaskets were used for all experiments. The holes acting as sample chambers were drilled into the pre-indented Re gaskets using an electric discharge machine. The maximum pressure reached in each experiment was dependent on the culet diameter and specific diamond anvil seat type. *In situ* pressures were measured using the calibrated shift of the R1 ruby fluorescence line,[38] and cross-referenced with the Ar-EoS [39] when possible. Five different compression runs were performed in total: Na_4Si_{24} compressed in Ar, Si_{24} compressed in Ar (twice), Si_{24} compressed in H_2, and Si_{24} compressed with no pressure medium (PM). The Na_4Si_{24} and Si_{24} samples were first crushed into fine powders and then pressed into pellets (~50 μm in diameter and 10-20 μm thick) before being loaded into the sample chambers. All gas loadings (Ar and H_2) were performed in-house, and were initially loaded to ~0.1 GPa. For the Si_{24} sample that was compressed without a PM, the crushed powder was inserted directly into the sample chamber, filling it almost entirely.

B. High-pressure X-ray diffraction and analysis

XRD measurements were performed at beamline 16-ID-B of the High-Pressure Collaborative Access Team (HPCAT), Advanced Photon Source, Argonne National Laboratory. A monochromatic X-ray beam with energy of ~30 keV and FWHM of approximately 4×6 μm^2 was focused on the sample.[40] The measurements

of Na_4Si_{24} (in Ar) and one Si_{24} experiment (in Ar) were collected on a 1-M Pilatus detector. The diffraction patterns from all other high-pressure experiments of Si_{24} (in Ar, H_2, and without a PM) were collected on a MAR-CCD detector. Samples were rotated in the beam from ω = -10° to 10° at 1°/s to improve powder averaging statistics. The sample-to-detector distance and other geometrical parameters were calibrated using Dioptas 0.5.0 [41] in conjunction with a CeO_2 diffraction standard. 2D diffraction images were processed using Dioptas 0.5.0, and Pawley refinements were performed using GSAS-II [42] to determine lattice parameters. In general, these refinements were performed on data ranging between 2θ = 3 – 16°, which includes approximately 50 Bragg peaks for either the Na_4Si_{24} or Si_{24} phases (see Supplementary Fig. 1). A polynomial background function was removed using GSAS-II, and Ar Bragg peaks were also fitted above the Ar solidification pressure. Typical estimated standard deviations on refined unit cell parameters were below 0.001 Å.

Zero-pressure bulk moduli (B_0) and their derivatives with respect to pressure (B_0') were determined using the EoSfit7c software [43] using both 3rd-order Birch–Murnaghan and Vinet equations of state. The uncertainty in V is determined from the GSAS-II LST output files, and the uncertainties in ruby pressure measurement are estimated to be ±2% for the experiments conducted in Ar and H_2, and ±5% for Si_{24} compressed with no PM. V_0 was set for all equation of state (EoS) refinements using the known values determined by powder-XRD at ambient conditions.

III. RESULTS AND DISCUSSION

Powder-XRD patterns were collected with increasing pressure for the five high-pressure experiments. Figure 2 shows select diffraction patterns of Si_{24} compressed in the H_2 PM up to 20.1 GPa. The signal diffracted from Si_{24} remains intense up to 18.0 GPa, before weakening substantially. During compression, all Si_{24} Bragg peaks shift to higher angle. Small variations in the relative intensities of Bragg peaks are due to small differences in powder averaging statistics between different locations in the cell (e.g., peaks between 2θ = 3 – 8°). Bragg peaks remain relatively sharp to the highest-pressure conditions, indicating that anisotropic strain broadening is not significant, and that the molecular H_2 PM provides quasi-hydrostatic compression conditions over the full range tested. While Si_{24} remains the dominant phase up to 18.0 GPa, clear signs of transformation toward other high-pressure Si phases are present, starting above 13 GPa. Bragg peaks from the β-Sn-Si phase were detected at 13.8 GPa, which transforms to the *Imma*-Si phase at 14.7 GPa. The *Imma*-Si phase persists alongside Si_{24} up to 17.3 GPa, above which simple-hexagonal (SH)-Si begins to form. The signal diffracted from SH-Si grows stronger as pressure is further increased, and by 20.1 GPa, the Si_{24} is almost completely gone, and the dominant phase is SH-Si.

The high-pressure phase transition sequence observed for Si_{24} perfectly mirrors that of compressed DC-Si with slight differences in the onset pressures and coexistence ranges. A recent precision study on compressed DC-Si in quasi-hydrostatic helium marks the β-Sn, *Imma*, and SH-Si onset pressures at 13.1, 13.1 and 15.5 GPa, respectively, with coexistence of the phases across the transition boundaries.[44] The similarity in the phase transition sequence between compressed DC-Si and Si_{24} reflects the strong thermodynamic driving force toward the denser phases at high pressure (volume drops ~20% across the β-Sn transition for DC-Si, even more for Si_{24}). Notably, DC-Si only persists to 13.1 GPa before transforming into denser phases. However, low-density Si_{24} can persist up to 20 GPa under similar quasi-hydrostatic conditions. The difference in this persistence under similar quasi-hydrostatic conditions might be related to

differences in kinetic barriers between the different starting allotropes. Previous phonon dispersion calculations predict that Si_{24} is dynamically stable to at least 10 GPa.[25]

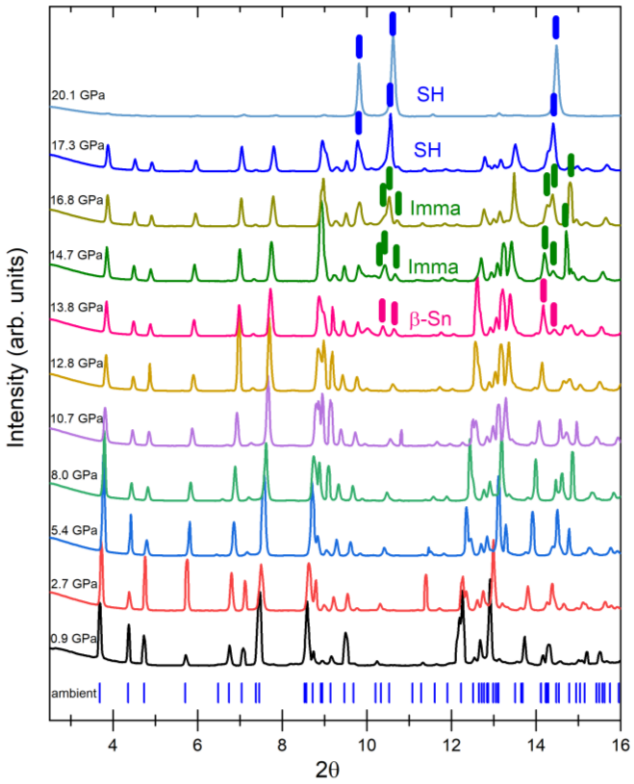

FIG. 2. Powder-XRD patterns of Si_{24} in a H_2 PM up to 20.1 GPa. Relative peak intensity variation is due to variations in powder averaging statistics. Other high-pressure Si phases such as β-Sn, *Imma* and SH-Si coexist alongside Si_{24} up to 20.1 GPa. Pink, green, and blue bars are used to indicate the peaks corresponding to β-Sn, *Imma* and SH-Si phases, respectively. The blue tick marks along the bottom indicate the Bragg peak positions for Si_{24} at ambient conditions.

The degree of hydrostaticity was found to influence Si_{24} phase transition and coexistence pressures, but did not affect the overall phase transition sequence, as summarized in Fig. 3. For the compression experiments performed in Ar (two combined datasets) and the experiment with no PM, the β-Sn-Si phase formed earlier relative to the experiment conducted in H_2, at 11.1 GPa and 11.3 GPa, respectively. The lower transition pressure is attributed to decreased hydrostaticity relative to H_2. Indeed, this behaviour is similar to observations for compressed DC-Si [45–47] and for Si_{136} clathrate compressed in less hydrostatic pressure media.[34] When compressed in Ar, β-Sn-Si (from Si_{24}) transforms to *Imma*-Si at 15.5 GPa, and then into SH-Si at 17.6 GPa. The Si_{24} experiment without a PM was stopped at 15 GPa, to prevent diamond-anvil culet damage.

In addition to having lower β-Sn-Si onset pressures, Si_{24} compressed in Ar and in no medium also persists to much lower pressures. As indicated by the thick black bars in Fig. 3, the highest pressure for which a refinable signal from Si_{24} was measured was only 13.2 GPa for Ar and 14.3 GPa for no PM. In contrast, Si_{24} compressed in H_2 yields a refinable diffraction pattern up to 18.0 GPa. These observations indicate that the Si_{24} phase transformation is facilitated by non-hydrostatic environments. It is also important to note that

DC-Si was never observed in any of the compression experiments. That is, the higher-pressure phases of Si form directly from compressed Si_{24} and not through an intermediate DC-Si phase.

Na_4Si_{24} compressed in Ar remained stable up to 18 GPa. However, unlike Si_{24} under the same conditions, no other higher-pressure Si phases were observed to co-exist. This indicates that the structure remains intact and Na remains in place within the Na_4Si_{24} channels up to at least 18 GPa, preventing the formation of localized regions of pure Si that are able to transform to other higher-pressure phases. Furthermore, even though the Na_4Si_{24} peaks remain visible up to 18 GPa, the decreased intensity of peaks in the diffraction patterns measured above 13.2 GPa makes it impossible to refine lattice parameters quantitatively. Other filled type-I [48] and type-III [49] Si clathrate structures have shown large homothetic volume collapses and irreversible amorphization at even higher pressures. For other chemical systems, this phenomenon typically occurs at lower pressures than their empty structural analogues.[50] However, our results show that this does not occur below 18 GPa for Na_4Si_{24} in an Ar PM. Experimental verification of these pressure thresholds is outside of the scope of this study.

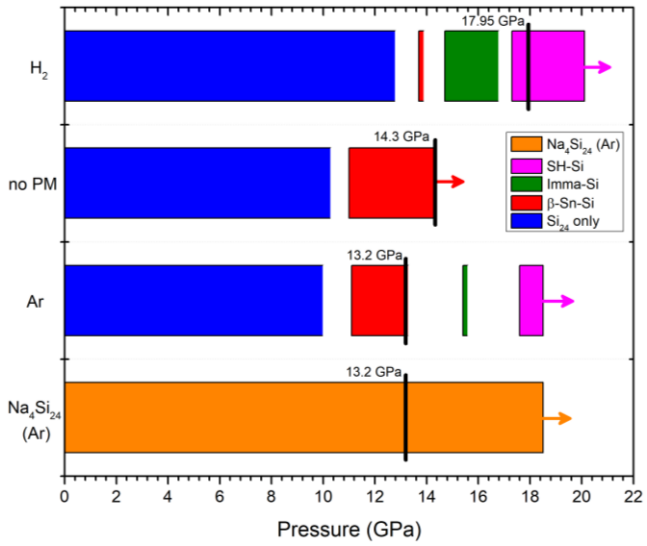

FIG. 3. A bar chart showing the observed phases of Si when Si_{24} and Na_4Si_{24} are compressed in different pressure media. The white spaces within each bar represent gaps in experimental pressures, where the phases on either side may exist. The onset pressure of the phase transformation from Si_{24} to β-Sn-Si is higher when compressed in H_2. Na_4Si_{24} persisted in Ar up to the highest pressure measured with no sign of co-existing high-pressure Si phases. The thick black lines indicate the highest pressure at which quantitative refinements of Si_{24} or Na_4Si_{24} could be made using GSAS-II. The arrows at the end of each bar indicate that the current phases may persist to higher pressures beyond what was measured.

Figure 4 shows the normalized decrease in the total unit cell volume (determined from refinement), V/V_0, with respect to pressure for Na_4Si_{24} in Ar, and for Si_{24} in Ar, H_2, and with no PM. A small variation in V_0 was observed for Na_4Si_{24} (~0.25%) between synchrotron data and our in-house measurement of the current sample, which is due to a small variation in a_0.[17] Notably, older samples (e.g., months after synthesis) exhibit smaller (up to 0.5%) values for a, consistent with Na-removal from the channels. It is known that

Na diffuses out of the channels very slowly over time at ambient conditions, [25,51] and could initially reflect a small decrease along the *a*-axis. While the compression curve reported here reflects one distinct sample composition near Na_4Si_{24}, we note that other slightly shifted curves may be possible due to small changes in stoichiometry, although further measurements are needed to confirm this hypothesis.

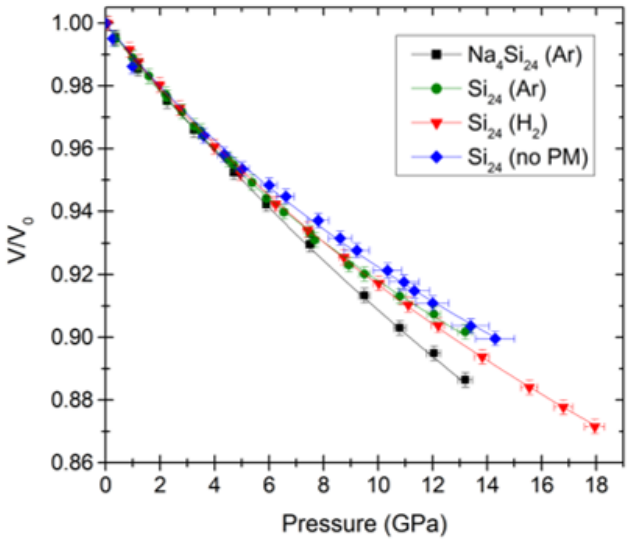

FIG. 4. The unit cell volume compression curves for Si_{24} in H_2 (red), Ar (green), and with no PM (blue), alongside that of Na_4Si_{24} in Ar (black). Uncertainties in volume measurements are taken from GSAS-II LST output files. Uncertainties in pressure are estimated to be higher for the sample measured with no PM. 3rd-order Birch–Murnaghan equations of state were determined using EoSfit7c and overlay their respective points on the plot. The uncertainties in both pressure and volume were taken into account during EoS fitting.

The compression curves presented in Fig. 4 show that Na_4Si_{24} is more compressible than Si_{24}. To determine the quantitative behavior, both 3rd-order Birch–Murnaghan and Vinet equations of state (EoS) were fitted to the compression data. The results are displayed in Table 1. For all compression curves, there is only a small difference between the values determined using each type of EoS. The B_0 of Na_4Si_{24} in Ar is 87(2) GPa and 86(2) GPa for the Birch–Murnaghan and Vinet fits, respectively. In both cases, B_0' determined from each fit is close to 4. The increased compressibility of Na_4Si_{24} relative to Si_{24} is attributed to its metallicity, which tends to decrease the directionality of covalent bonds and overall rigidity of the framework. For the case of Na_4Si_{24}, the Na valence electrons are donated to silicon framework rendering the system metallic, whereas Si_{24} possesses a balanced electron count and band gap near 1.4 eV. Further to this, the results showing that the Na-filled structure has a lower B_0 than empty Si_{24} is expected. A similar trend has previously been observed for silicon clathrates [52] and has been predicted for carbon clathrates.[53]

When compressed in quasi-hydrostatic H_2, B_0 for Si_{24} is 91(2) GPa for both the Birch–Murnaghan and Vinet EoS. At ambient conditions, the Si-Si bond lengths within the open-framework structure of Si_{24} range from 2.33-2.41 Å and the bond angles vary between 93.7-139.5°, in comparison with bond lengths and bond angles in the perfectly tetrahedral DC-Si structure that are 2.35 Å and 109.5°, respectively. Also, the density of Si_{24} is substantially lower than that of DC-Si, at 2.17 g/cm^3 relative to 2.33 g/cm^3.[25] These structural factors make it no surprise that Si_{24} is more compressible than DC-Si (B_0 = 97.9 GPa and B_0' = 4.24).[44] The

lower B_0 of 91(2) GPa for Si_{24} compressed in H_2 scales well with the reduction in density compared with DC-Si (~7%), and is similar to that of other open-framework or polyhedral Si structures with distorted bond lengths and angles. For example, the Si_{136} structure which has a density of 2.15 g/cm^3, was shown to have a B_0 of 90(5) GPa,[34] similar to Si_{24}. The B_0' value determined for Si_{24} in H_2 is larger than that of DC-Si (4.2 GPa [44]), and consistent with the larger initial volume reduction of the open-framework structure.

The fact that the compression curve of Si_{24} compressed in H_2 is nearly identical to that of Si_{24} in Ar and with no PM suggests that H_2 is not able to enter the structure in the pressure range investigated, as has been proposed previously as a possibility.[54] If H_2 was able to enter the structure, we would expect to see an abrupt stiffening or flattening of the compression curve, as observed when small molecules penetrate the pores of other open-framework systems.[55–58] We find no evidence for H_2 incorporation under room temperature compression, although cannot fully exclude some nominal amount of penetration into the structure. A previous Raman study conducted at high pressure and high temperature also indicates that He penetration is unlikely up to 8 GPa and 400 K.[33]

Table 1. Bulk moduli, B_0, and their derivatives, B_0', with respect to pressure for Na_4Si_{24} in Ar, and for Si_{24} in H_2, Ar, and with no PM. Estimated uncertainties in the last digit are shown in parentheses, as determined from EoSfit7c. For all EoS fitting results shown here, V_0 was set to 515.87(5) Å for Si_{24} and at 529.95(5) Å for Na_4Si_{24}, as determined from powder-XRD measurements.

	3rd-order Birch–Murnaghan EoS		Vinet EoS	
Sample (PM)	B_0 (GPa)	B_0'	B_0 (GPa)	B_0'
Na_4Si_{24} (Ar)	87(2)	4.1(6)	86(2)	4.2(6)
Si_{24} (Ar)	86(2)	7.3(7)	86(2)	7.3(6)
Si_{24} (H_2)	91(2)	5.3(5)	91(2)	5.4(4)
Si_{24} (no PM)	88(3)	9(1)	89(3)	8(1)

Relative to compression in H_2, B_0 of Si_{24} appears lower when compressed without a PM up to 14 GPa, and even more so when compressed in Ar up to 13.2 GPa. For both of these data sets, the best-fit B_0' values are significantly higher. These trends hold for both the Birch–Murnaghan and Vinet EoS and demonstrate the role of hydrostaticity on compression. For comparison, the F-f plots of Si_{24} and Na_4Si_{24} in Ar, and Si_{24} in H_2 generated in Eosfit7c using the Birch-Murnaghan EoS are shown in supplementary Figs. 2-4, respectively. Indeed, previous studies have documented how non-hydrostatic conditions can affect the EoS for many systems, including Si.[44] The compression curves for Si_{24} in all cases appear similar at low pressure, but begin to deviate at higher pressure. In the absence of a PM, a clear offset begins above ~5 GPa when compared with quasi-hydrostatic H_2. Excluding the highest-pressure Ar points in the refinement yields EoS parameters that are in much better agreement with the case of H_2 (Table 1). We attribute these differences to the loss of hydrostaticity with increasing pressure. The (quasi)hydrostatic limit of Ar was previously shown to persist to about 9 GPa.[59] As mentioned above, we attribute the differences in phase transition pressures shown in Fig. 3 directly to these differences in hydrostaticity. Previous studies on high-pressure transformations in pure Si have also shown strong dependencies on hydrostaticity.[44]

While the volumetric compressibilities of Na_4Si_{24} and Si_{24} exhibit similar trends with their bulk moduli differing by ~7%, it is interesting to examine the behavior of individual lattice parameters and structural

compression mechanisms. Figure 5 highlights the behavior of *a*, *b*, and *c* for both Na_4Si_{24} and Si_{24} with respect to pressure. While the general trends for Si_{24} are consistent for all pressure media conditions (with small deviations attributed to the non-hydrostaticity discussed previously), it is also clear that Si_{24} and Na_4Si_{24} exhibit fundamentally different behavior along different crystallographic axes. Na_4Si_{24} is much more compressible in both the *b* and *c* directions, while it is much less compressible along the *a* direction. This behavior can be understood by the fact that channels in the structure propagate along the *a*-axis, and, when filled with Na ions, provide strong resistance to compression in this direction. Despite showing decreased compressibility along *a*, the overall increase in volumetric compressibility of Na_4Si_{24} is due to more compressible *b* and *c* axes, as compared with Si_{24}.

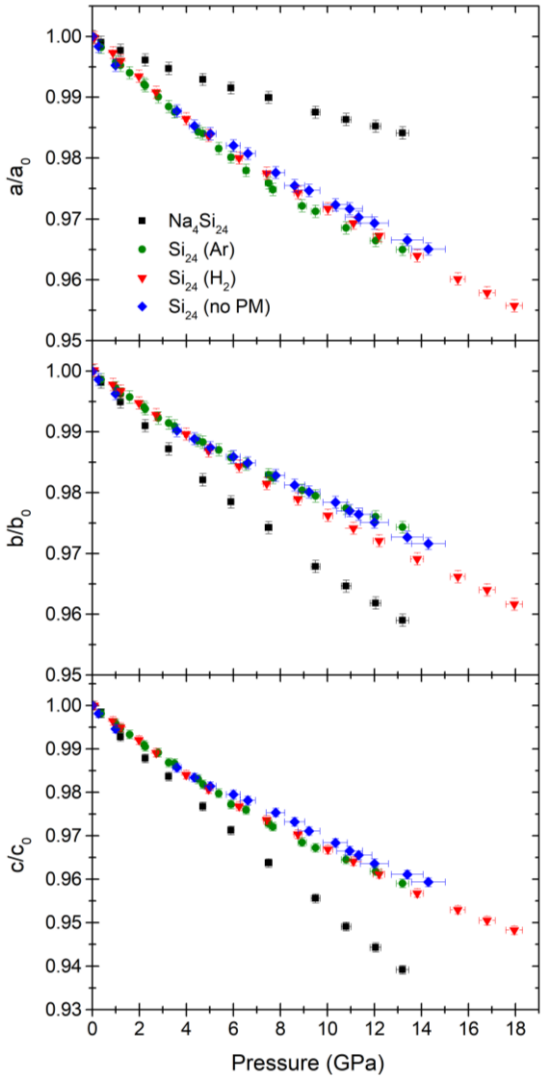

FIG. 5. The compression curves of the *a*, *b*, and *c* unit cell parameters with respect to pressure of Si_{24} in H_2 (red), Ar (green), and with no PM (blue), alongside that of Na_4Si_{24} in Ar (black). Uncertainties in in the refined unit cell parameters are taken from GSAS-II LST output files. Uncertainties in pressure are estimated to be higher for the sample measured with no PM.

In all cases, the individual lattice parameters decrease monotonically over the entire pressure range tested, with no indication of negative linear compressibility at room temperature. The determination of B_0 for Si_{24} allows for accurate determinations of mode Grüneisen parameters from high-pressure Raman spectroscopy, which previously assumed B_0 = 90 GPa.[33] The observation of negative Grüneisen parameters for Si_{24} may indicate the possibility for low-temperature negative thermal expansion, as was observed previously for Si_{136}, [30] motivating future studies on Si_{24} over a broader range of pressure and temperature conditions.

IV. CONCLUSION

In this work we experimentally determined B_0 and B_0' for and Si_{24} and Na_4Si_{24} under quasi- and non-hydrostatic high-pressure conditions. EoS fits of compression curves show that the B_0 of Si_{24} compressed in H_2 is 91(2) GPa, which is ~7% lower than the denser DC-Si structure, and is comparable to the B_0 of other open-framework Si allotropes, such as Si_{136}. The compression curves also show that Si_{24} compressed in H_2 and without a PM vary only subtly, suggesting that H_2 does not enter the Si_{24} structure under high pressure at room temperature. Both Si_{24} and Na_4Si_{24} structures exhibit comparable volumetric compressibilities, however there are differing axial trends, such as Na_4Si_{24} having a significantly higher incompressibility along the *a*-axis due to Na-filled channels along this direction. High-pressure XRD patterns reveal that the Na_4Si_{24} structure persists up to at least 18 GPa. Whereas, Si_{24} partially transforms into high-pressure phases including β-Sn, *Imma* and SH-Si, but is able to co-exist alongside these phases. The results also show that the Si_{24} to β-Sn-Si pressure transformation threshold depends strongly on the choice of PM, and that the transformation is suppressed in more hydrostatic environments.

V. ACKNOWLEDGEMENTS

The authors gratefully acknowledge Dr Michael Guerette, Dr Haidong Zhang, Dr Stevce Stefanoski, and Dr Oleksandr Kurakevych for their contributions toward materials synthesis, Dr Piotr Gunka for guidance with data analysis and refinement, and Dr Yue Meng for assistance during the HPCAT beamtimes. This work was supported by the National Science Foundation, Division of Material Research (NSF-DMR) under award number 1809756. Portions of this work were performed at HPCAT (Sector 16), Advanced Photon Source (APS), Argonne National Laboratory. HPCAT operations are supported by DOE-NNSA's Office of Experimental Sciences. The Advanced Photon Source is a U.S. Department of Energy (DOE) Office of Science User Facility operated for the DOE Office of Science by Argonne National Laboratory under Contract No. DE-AC02-06CH11357

VI. REFERENCES

[1] M.S. Hybertsen and S.G. Louie, Phys. Rev. Lett. **55**, 1418 (1985).

[2] M.A. Green, Sol. Energy Mater. Sol. Cells **92**, 1305 (2008).

[3] T.N. Theis and P.M. Solomon, Science. **327**, 1600 (2010).

[4] W.L. Ng, M.A. Lourenc, R.M. Gwilliam, S. Ledain, G. Shao, and K.P. Homewood, Nature **410**, 192 (2001).

[5] S. Botti, J.A. Flores-Livas, M. Amsler, S. Goedecker, and M.A.L. Marques, Phys. Rev. B **86**, 121204 (2012).

[6] M. Fujita, Nat. Photonics **7**, 264 (2013).

[7] S. Barth, M.S. Seifner, and S. Maldonado, Chem. Mater. **32**, 2703 (2020).

[8] B. Haberl, J.E. Bradby, and T.A. Strobel, Appl. Phys. Rev. **3**, 040808 (2016).

[9] L. Rapp, B. Haberl, C.J. Pickard, J.E. Bradby, E.G. Gamaly, J.S. Williams, and A. V. Rode, Nat. Commun. **6**, 7555 (2015).

[10] B.D. Malone, J.D. Sau, and M.L. Cohen, Phys. Rev. B **78**, 035210 (2008).

[11] H. Zhang, H. Liu, K. Wei, O.O. Kurakevych, Y. Le Godec, Z. Liu, J. Martin, M. Guerrette, G.S. Nolas, and T.A. Strobel, Phys. Rev. Lett. **118**, 146601 (2017).

[12] J.M. Besson, E.H. Mokhtari, J. Gonzalez, and G. Weill, Phys. Rev. Lett. **59**, 473 (1987).

[13] J.S. Kasper and R.H. Wentorf, Science. **197**, 599 (1977).

[14] E.M.T. Fadaly, A. Dijkstra, J.R. Suckert, D. Ziss, M.A.J. van Tilburg, C. Mao, Y. Ren, V.T. van Lange, K. Korzun, S. Kölling, M.A. Verheijen, D. Busse, C. Rödl, J. Furthmüller, F. Bechstedt, J. Stangl, J.J. Finley, S. Botti, J.E.M. Haverkort, and E.P.A.M. Bakkers, Nature **580**, 205 (2020).

[15] M. Beekman, S.M. Kauzlarich, L. Doherty, and G.S. Nolas, Materials (Basel). **12**, 1139 (2019).

[16] J.S. Kasper, P. Hagenmuller, M. Pouchard, and C. Cros, Science. **150**, 1713 (1965).

[17] O.O. Kurakevych, T.A. Strobel, D.Y. Kim, T. Muramatsu, and V. V. Struzhkin, Cryst. Growth Des. **13**, 303 (2013).

[18] Z. Jouini, O. Kurakevych, H. Moutaabbid, Y. Le Godec, M. Mezouar, and N. Guignot, J. Superhard Mater. **38**, 66 (2016).

[19] J. Gryko, P.F. McMillan, R.F. Marzke, G.K. Ramachandran, D. Patton, S.K. Deb, and O.F. Sankey, Phys. Rev. B **62**, R7707 (2000).

[20] A. Ammar, C. Cros, M. Pouchard, N. Jaussaud, J.M. Bassat, G. Villeneuve, M. Duttine, M. Ménétrier, and E. Reny, Solid State Sci. **6**, 393 (2004).

[21] T. Narita, H. Ueno, T. Baba, T. Kume, T. Ban, T. Iida, H. Habuchi, H. Natsuhara, and S. Nonomura, Phys. Status Solidi **7**, 1200 (2010).

[22] F. Ohashi, Y. Iwai, A. Noguchi, T. Sugiyama, M. Hattori, T. Ogura, R. Himeno, T. Kume, T. Ban, and S. Nonomura, J. Phys. Chem. Solids **75**, 518 (2014).

[23] J.D. Bryan and G.D. Stucky, Chem. Mater. **13**, 253 (2001).

[24] M. Guerette, M.D. Ward, K.A. Lokshin, A.T. Wong, H. Zhang, S. Stefanoski, O. Kurakevych, Y. Le Godec, S.J. Juhl, N. Alem, Y. Fei, and T.A. Strobel, Cryst. Growth Des. **18**, 7410 (2018).

[25] D.Y. Kim, S. Stefanoski, O.O. Kurakevych, and T.A. Strobel, Nat. Mater. **14**, 169 (2015).

[26] M. Guerette, M.D. Ward, L. Zhu, and T.A. Strobel, J. Phys. Condens. Matter **32**, 194001 (2020).

[27] J. Linghu, L. Shen, M. Yang, S. Xu, and Y.P. Feng, J. Phys. Chem. C **121**, 15574 (2017).

[28] W. Shockley and H.J. Queisser, J. Appl. Phys. **32**, 510 (1961).

[29] K. Momma and F. Izumi, J. Appl. Crystallogr. **44**, 1272 (2011).

[30] X. Tang, J. Dong, P. Hutchins, O. Shebanova, J. Gryko, P. Barnes, J.K. Cockcroft, M. Vickers, and P.F. McMillan, Phys. Rev. B **74**, 014109 (2006).

[31] T.A. Mary, J.S.O. Evans, T. Vogt, and A.W. Sleight, Science. **272**, 90 (1996).

[32] W. Miller, C.W. Smith, D.S. MacKenzie, and K.E. Evans, J. Mater. Sci. **44**, 5441 (2009).

[33] X. Tong, X. Xu, B. Fultz, H. Zhang, T.A. Strobel, and D.Y. Kim, Phys. Rev. B **95**, 094306 (2017).

[34] A. San-Miguel, P. Kéghélian, X. Blase, P. Mélinon, A. Perez, J.P. Itié, A. Polian, E. Reny, C. Cros, and M. Pouchard, Phys. Rev. Lett. **83**, 5290 (1999).

[35] H. Takizawa, K. Miura, M. Ito, T. Suzuki, and T. Endo, J. Alloys Compd. **282**, 79 (1999).

[36] N.E.R. Zimmermann, M. Haranczyk, M. Sharma, B. Liu, B. Smit, and F.J. Keil, Mol. Simul. **37**, 986 (2011).

[37] E. Cohen De Lara and R. Kahn, Zeolites **12**, 256 (1992).

[38] H.K. Mao, J. Xu, and P.M. Bell, J. Geophys. Res **91**, 4673 (1986).

[39] D. Errandonea, R. Boehler, S. Japel, M. Mezouar, and L.R. Benedetti, Phys. Rev. B **73**, 092106 (2006).

[40] G. Shen, P. Chow, Y. Xiao, S. Sinogeikin, Y. Meng, W. Yang, H.P. Liermann, O. Shebanova, E. Rod, A. Bommannavar, and H.K. Mao, High Press. Res. **28**, 145 (2008).

[41] C. Prescher and V.B. Prakapenka, High Press. Res. **35**, 223 (2015).

[42] B.H. Toby and R.B. Von Dreele, J. Appl. Crystallogr. **46**, 544 (2013).

[43] R.J. Angel, J. Gonzalez-Platas, and M. Alvaro, Zeitschrift Fur Krist. **229**, 405 (2014).

[44] S. Anzellini, M.T. Wharmby, F. Miozzi, A. Kleppe, D. Daisenberger, and H. Wilhelm, Sci. Rep. **9**, 15537 (2019).

[45] H. Olijnyk, S.K. Sikka, and W.B. Holzapfel, Phys. Lett. **103A**, 137 (1984).

[46] J.Z. Hu, L.D. Merkle, C.S. Menoni, and I.L. Spain, Phys. Rev. B **34**, 4679 (1986).

[47] M.I. McMahon, R.J. Nelmes, N.G. Wright, and D.R. Allan, Phys. Rev. B **50**, 739 (1994).

[48] A.S. Miguel, A. Merlen, P. Toulemonde, T. Kume, S. Le Floch, A. Aouizerat, S. Pascarelli, G. Aquilanti, O. Mathon, T. Le Bihan, J.P. Itié, and S. Yamanaka, Europhys. Lett. **69**, 556 (2005).

[49] P. Toulemonde, D. MacHon, A. San Miguel, and M. Amboage, Phys. Rev. B - Condens. Matter Mater. Phys. **83**, 134110 (2011).

[50] A. San-Miguel and P. Toulemonde, High Press. Res. **25**, 159 (2005).

[51] U. Arrieta, N.A. Katcho, O. Arcelus, and J. Carrasco, Sci. Rep. **7**, 5350 (2017).

[52] D. MacHon, P. Toulemonde, P.F. McMillan, M. Amboage, A. Muñoz, P. Rodríguez-Hernández, and A. San Miguel, Phys. Rev. B - Condens. Matter Mater. Phys. **79**, 184101 (2009).

[53] N. Rey, A. Muñoz, P. Rodríguez-Hernndez, and A. San Miguel, J. Phys. Condens. Matter **20**, 215218 (2008).

[54] Y. Bi, E. Xu, T.A. Strobel, and T. Li, Commun. Chem. **1**, 15 (2018).

[55] R.M. Hazen and L.W. Finger, J. Appl. Phys. **56**, 1838 (1984).

[56] M. Colligan, P.M. Forster, A.K. Cheetham, Y. Lee, T. Vogt, and J.A. Hriljac, J. Am. Chem. Soc. **126**, 12015 (2004).

[57] K. Niwa, T. Tanaka, M. Hasegawa, T. Okada, T. Yagi, and T. Kikegawa, Microporous Mesoporous Mater. **182**, 191 (2013).

[58] G.D. Gatta, P. Lotti, and G. Tabacchi, Phys. Chem. Miner. **45**, 115 (2018).

[59] S. Klotz, J.-C. Chervin, P. Munsch, and G. Le Marchand, J. Phys. D Appl. Phys. **42**, 075413 (2009).